minerals

MDPI

Article

Optimizing Confined-Turbulence Conditioning for Enhanced Flotation of Coal Gasification Fine Slag

Shuping Yang [1,2,3,†], Xiaoheng Li [1,2,3,†], Danlong Li [1,2,3,4], Haochun Hou [1,2,3], Jincai Ran [1,2,3,5], Xiaokang Yan [1,2,3], Haijun Zhang [1,2,3,*] and Hainan Wang [1,2,3,*]

1 State Key Laboratory of Coking Coal Resources Green Exploitation, China University of Mining and Technology, Xuzhou 221116, China; 15263764520@163.com (S.Y.); lixiaoheng0221@163.com (X.L.)
2 Chinese National Engineering Research Center of Coal Preparation and Purification, China University of Mining and Technology, Xuzhou 221116, China
3 School of Chemical Engineering and Technology, China University of Mining and Technology, Xuzhou 221116, China
4 School IMDEA Nanociencia, C/Faraday 9, 28049 Madrid, Spain
5 School of Mining Engineering and Geology, Xinjiang Institute of Engineering, Urumqi 830023, China
* Correspondence: zhjcumt@163.com (H.Z.); wanghainan07@163.com (H.W.)
† These authors contributed equally to this work.

Abstract

Coal gasification fine slag (CGFS), a major solid by-product of coal gasification, contains substantial unburned carbon. However, efficient carbon–ash separation during CGFS flotation is often restricted by its complex surface properties. This study aims to enhance the flotation performance of CGFS by introducing a confined-turbulence pulp conditioning system. To clarify the role of conditioning pretreatment, the coupled effects of conditioning time and hydrodynamic intensity were systematically investigated. Flotation experiments were conducted to compare the separation performance under different conditions. Additionally, collector adsorption tests, wrap-angle measurements, zeta-potential analysis, and X-ray photoelectron spectroscopy (XPS) were performed to reveal the underlying interfacial modification mechanisms. The results indicate that within an appropriate time window, the intensified turbulence and high shear forces can effectively remove surface impurities and strengthen particle–reagent collision and adhesion, thereby improving flotation selectivity and combustible recovery. Specifically, an optimal conditioning time of 80 s achieves the maximum combustible recovery. Conversely, excessive conditioning induces an over-shearing effect, which leads to reagent desorption and a subsequent deterioration in flotation performance. In conclusion, the confined-turbulence pulp conditioning strategy successfully restructures the surface properties of CGFS and enhances its flotation efficiency. These findings provide fundamental data and a feasible technical approach for intensifying the carbon–ash separation of CGFS.

Keywords: flotation; pulp conditioning; coal gasification fine slag; turbulence; conditioning time

Check for updates

Academic Editor: Mehmet Sabri Celik

Received: 2 February 2026
Revised: 10 March 2026
Accepted: 10 March 2026
Published: 13 March 2026

Copyright: © 2026 by the authors. Licensee MDPI, Basel, Switzerland. This article is an open access article distributed under the terms and conditions of the Creative Commons Attribution (CC BY) license.

1. Introduction

For the foreseeable future, coal is destined to maintain its dominant position in China's energy system, fueled by a fundamental resource reality: the country is coal-rich but oil-deficient and gas-limited [1,2]. Driven by the national dual-carbon strategy, the clean and efficient utilization of coal has emerged as a significant goal for energy development. In this scenario, coal gasification—a process that catalytically converts coal into syngas

under controlled temperature and pressure within an oxygen-containing atmosphere—has been established as a key technological pathway towards achieving efficient and clean coal conversion [3–5]. Coal gasification slag is a solid residue from incomplete physicochemical reactions. It is categorized as either coarse or fine slag based on discharge mode. The former is primarily inorganic, whereas the latter contains both residual carbon and inorganic minerals, with a markedly higher carbon content [6–9]. With the rapid expansion of the coal gasification industry, the resource-oriented utilization of coal gasification slag has become an urgent and critical issue, among which the effective separation and recovery of residual carbon from coal gasification fine slag (CGFS) constitutes a particularly important challenge [10–13].

In the mineral processing field, methods for separating unburned carbon from CGFS typically include screening, gravity concentration, flotation, and chemical separation. Among these, froth flotation, a typical physicochemical separation technique based on differences in particle surface wettability, is widely recognized as one of the most effective methods for recovering valuable components from fine solid wastes. According to classic flotation theory, hydrophobic unburned carbon particles selectively collide with and attach to air bubbles, subsequently rising to the froth zone, while hydrophilic ash minerals remain dispersed in the aqueous pulp. In practical industrial applications, flotation technology has been extensively implemented in mineral processing and coal preparation, playing a vital role in secondary resource recovery, environmental remediation, and the promotion of green and smart mining engineering [14]. Under conventional flotation conditions, the decarbonization of coal gasification fine slag typically requires a kerosene dosage of 6–25 kg/t, while the combustible recovery of residual carbon generally remains around 80%. This reflects the challenges of excessive reagent consumption and limited recovery efficiency in CGFS flotation [13,15,16]. This is determined by the intrinsic properties of CGFS. CGFS is characterized by complex composition and fine particle size. The particle surfaces are often enriched with oxygen-containing functional groups such as C–O and C=O, as well as mineral impurities like SiO_2, which cause the particle surfaces to exhibit strong hydrophilicity. As a result, flotation reagents cannot effectively adsorb and spread on the particle surface, greatly reducing the interaction between the particles and the reagents. To enhance the carbon–ash separation efficiency of CGFS during flotation, extensive studies have been conducted [17–20]. Xue et al. [21] improved CGFS flotation by formulating a composite collector composed of kerosene and dodecylamine polyoxyethylene ether, and the results indicated that the addition of the surfactant effectively reduced the dispersion size of kerosene droplets, thereby enhancing carbon–ash separation. Yang et al. [22] employed ultrasonic pretreatment to induce changes in the surface chemical properties of CGFS, whereby the content of hydrophilic functional groups on particle surfaces decreased, leading to enhanced surface hydrophobicity and improved flotation performance. Lv et al. [10] adopted a combined gravity separation–flotation process, in which gravity separation of CGFS was first employed for preliminary enrichment, followed by grinding of the concentrates and subsequent flotation, ultimately achieving efficient separation of carbon and ash components.

For the flotation process, effectively improving particle surface properties and enhancing the difference in floatability between carbonaceous and ash particles are the keys to achieving efficient separation of carbon and ash components in CGFS. The conditioning pretreatment prior to flotation generates a turbulent flow field inside the conditioning device through mechanical agitation, under which a scrubbing effect is exerted on the CGFS particle surfaces, removing previously attached high-ash slimes, and reducing the content of oxygen-containing functional groups, thereby effectively enhancing the surface hydrophobicity of unburned carbon. As a result, the collision probability and adsorption

between particles and reagents will be increased, enabling effective surface modification of particles and ultimately amplifying the floatability difference between carbon and ash particles [23,24]. At present, the development and application of conditioning equipment mainly focus on increasing energy input and performing structural optimization. Enhancement of energy input is typically achieved by increasing the external energy during the conditioning process to improve energy utilization and transfer within the device, whereas structural optimization aims to improve the internal flow-field characteristics by designing the internal geometry to construct multi-regime turbulent flow environments, thereby strengthening particle dispersion uniformity and selective adsorption of collectors [25–28]. Yu et al. [29] reported that increasing energy input during agitation could effectively enhance the scrubbing effect on particle surfaces and intensify interactions with reagents; Yang et al. [30] optimized the impeller structure and developed a fractal impeller to intensify the conditioning process, significantly improving particle surface modification and flotation performance; Chen et al. [23] developed a colliding-flow conditioning device, and comparative characterization and flotation experiments under different feeding flow rates demonstrated that increasing the feeding flow rate could effectively enhance conditioning performance.

Building upon previous studies on the optimization of pulp conditioning machines, a confined-turbulence pulp conditioning machine (CTPCM) was designed and constructed in this work. The machine integrates the synergistic action of a three-way impinging jet feed, internal multistage impeller agitation, and baffles to establish a high-turbulence, high-shear flow field favorable for flotation, thereby enhancing effective contact between particles and reagents in the slurry, promoting particle surface modification, and ultimately intensifying the flotation separation process of CGFS. In prior work, our research group [31] systematically evaluated the influence of impeller rotational speed on the structure and characteristics of the confined turbulent flow field, clarifying the optimal speed range and the role of energy input in intensifying the flotation process. This follow-on study examines feeding flow rate as a principal control variable to explore whether an optimal conditioning window exists for the flotation of coal gasification fine slag in a confined turbulent conditioning device. The feeding flow rate directly affects jet collision velocity and slurry residence time during conditioning. By comparatively analyzing the characterization results and flotation performance of samples conditioned at different feeding flow rates, the intensification effects of the feeding flow rate on particle surface modification and flotation selectivity were systematically verified.

2. Experimental

2.1. Experimental Apparatus

A confined-turbulence pulp conditioning machine (CTPCM) was developed in this study, and a conditioning system for CGFS was constructed. The conditioning equipment has a total height of 300 mm and a cylindrical body diameter of 200 mm. Three feeding pipes are arranged 30 mm above the bottom of the cylinder and axially distributed at intervals of 120°, each with an inner diameter of 14 mm. Two annular baffles are installed inside the cylinder at distances of 52 mm and 173 mm from the bottom, with inner diameters of 50 mm for the lower annular baffle and 90 mm for the upper annular baffle. Additionally, four side baffles are uniformly distributed along the inner wall of the cylinder at 90° intervals. The stirring shaft has a length of 200 mm and is equipped with three impellers: the upper impeller is a dispersing impeller to ensure slurry circulation within the cylinder, the middle impeller is a forced impeller that provides strong shear to effectively scrub particle surfaces, and the lower impeller is a pumping impeller that promotes slurry transport and enhances the dispersion of particles and reagents in the slurry. The photograph of the conditioning

machine is shown in Figure 1. During operation, the slurry is driven by the feed pump from the circulation tank and divided into three streams by a distributor, which are uniformly fed into the three colliding pipes to generate high-velocity impinging flows inside the machine; meanwhile, the stirring shaft drives the multistage impellers to rotate, and the slurry ascends through the cylinder, undergoing multistage impeller agitation and turbulent flow-field action before being discharged from the top outlet, thereby completing the conditioning process. During the conditioning process, the feeding flow rate was adjusted by regulating the frequency of the feed pump, while the impeller speed was maintained constant at 2000 rpm.

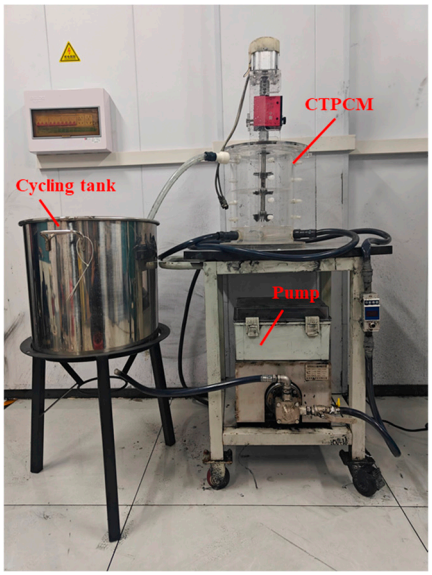

Figure 1. Schematic diagram of the CTPCM system.

In this study, the feeding flow rate is treated as an integrated operational variable to represent the coupled effects of residence time and hydrodynamic intensity. Variations in the feeding flow rate simultaneously influence jet collision velocity and slurry residence time, thereby affecting the overall conditioning environment.

2.2. Experimental Samples

The CGFS sample used in this study was obtained from a coal-to-liquids gasification process. Prior to sampling, the coning and quartering method was applied for pretreatment to ensure the representativeness of the experimental sample. Proximate and ultimate analyses were conducted on the gasification slag sample, and the results are presented in Table 1. The proximate analysis was performed using an automatic proximate analyzer (XL-2000, Hebi Keda Instrument Co., Ltd., Hebi, China), yielding a moisture content of 1.41%, an ash content of 74.80%, a volatile matter content of 3.62%, and a fixed carbon content of 20.17%. Ultimate analysis was carried out using an elemental analyzer (UNICUBE, Elementar Analysensysteme GmbH, Langenselbold, Germany). The contents of carbon, hydrogen, sulfur, and oxygen are 22.56%, 0.57%, 0.15%, and 76.60%, respectively.

Table 1. Proximate and ultimate analyses of coal gasification fine slag.

Proximate Analysis (ad, %)				**Ultimate Analysis (ad, %)**				
M_{ad}	A_{ad}	V_{ad}	FC_{ad} [#]	N_{ad}	C_{ad}	H_{ad}	S_{ad}	O_{ad} [#]
1.41	74.80	3.62	20.17	0.12	22.56	0.57	0.15	76.60

ad: air dry basis; [#]: by difference subtraction calculation.

The particle size distribution of the raw sample is presented in Table 2. The sample exhibited a relatively coarse size distribution. To satisfy the particle size requirements for subsequent flotation experiments, grinding tests were conducted on the sample prior to flotation. The experimental samples were obtained by grinding in a laboratory rod mill at 400 rpm for 10 min. Particle size analysis was performed using a laser particle size analyzer (Mastersizer 3000, Malvern Panalytical, Malvern, UK). The final particle size test results are shown in Figure 2. As depicted, particles smaller than 67.85 μm accounted for 90% of the experimental sample, while those smaller than 19.77 μm constituted 50%. Overall, the particle size distribution was relatively fine.

Table 2. Particle size analysis of the raw coal gasification fine slag sample.

Particle Size/mm	Yield/%	Ash/%	Cumulative Above		Cumulative Undersize	
			Yield/%	Ash/%	Yield%	Ash/%
+0.5	5.82	90.11	5.82	90.11	100.00	74.67
0.5–0.25	14.54	87.54	20.36	88.27	94.18	73.71
0.25–0.125	11.25	71.24	31.61	82.21	79.64	71.19
0.125–0.074	14.32	67.31	45.93	77.57	68.39	71.18
0.074–0.045	8.76	80.42	54.69	78.02	54.07	72.21
−0.045	45.31	70.62	100.00	74.67	45.31	70.62
Total	100.00	74.67				

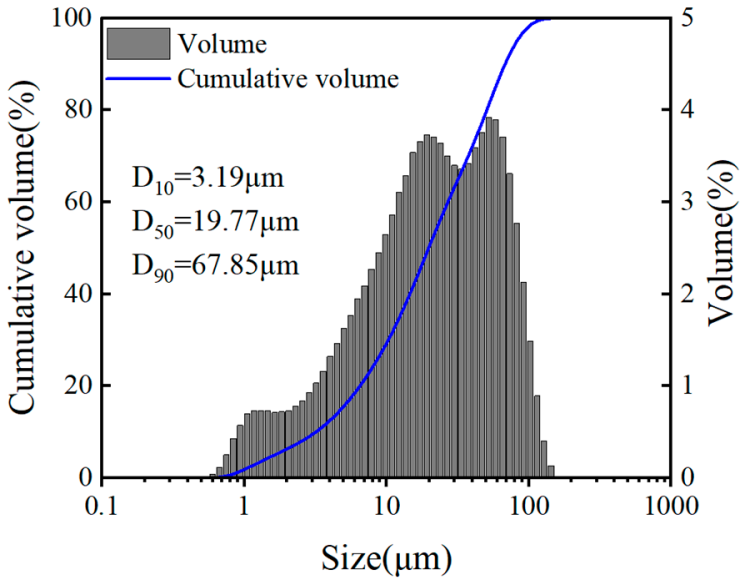

Figure 2. Particle size analysis of coal gasification fine slag.

X-ray diffraction (XRD) analysis was conducted to identify the mineralogical composition of the CGFS sample, and the corresponding results are shown in Figure 3. The XRD pattern exhibits a pronounced characteristic peak of quartz at $2\theta \approx 26.9^\circ$ (labeled Q), indicating that the sample contains a substantial amount of crystalline quartz, which is mainly derived from quartz particles in the raw coal that did not participate in the gasification reactions and subsequently recrystallized during the cooling process. Furthermore, a distinct broad diffuse hump in the 20–40° range is observed, suggesting the presence of substantial amorphous phases, which can be attributed to the amorphous carbon contained in the CGFS.

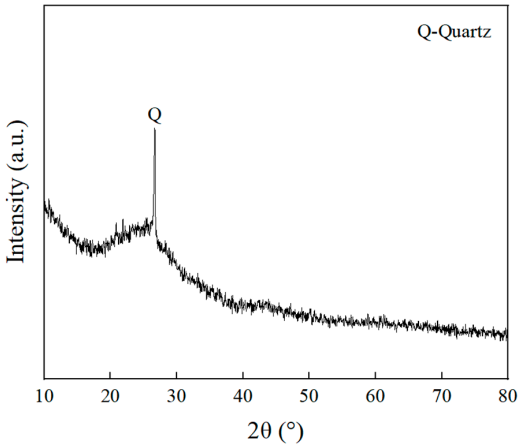

Figure 3. XRD pattern of coal gasification fine slag.

Scanning electron microscopy (SEM) combined with energy-dispersive X-ray spectroscopy (EDS) was employed to characterize the surface morphology and elemental distribution of the CGFS sample, and the results are presented in Figure 4. As shown in Figure 4a, the CGFS sample consists of flocculent particles, spherical particles, and adhered particles, with pronounced intermixing, attachment, and encapsulation among the different morphologies. Region (I) is mainly composed of spherical particles, and the corresponding locally magnified morphology is shown in Figure 4b. The EDS spectrum in Figure 4d indicates that the spherical particles are dominated by Si and O, suggesting that they are primarily silicon oxides, while a portion of residual carbon particles is adhered to their surfaces. Region (II) is mainly composed of flocculent particles, and the locally magnified morphology is shown in Figure 4c. The EDS spectrum in Figure 4e reveals that the flocculent particles are rich in C with minor amounts of Si and O, indicating that they consist predominantly of residual carbon, accompanied by a certain amount of silicon oxides adhered to the carbon surfaces.

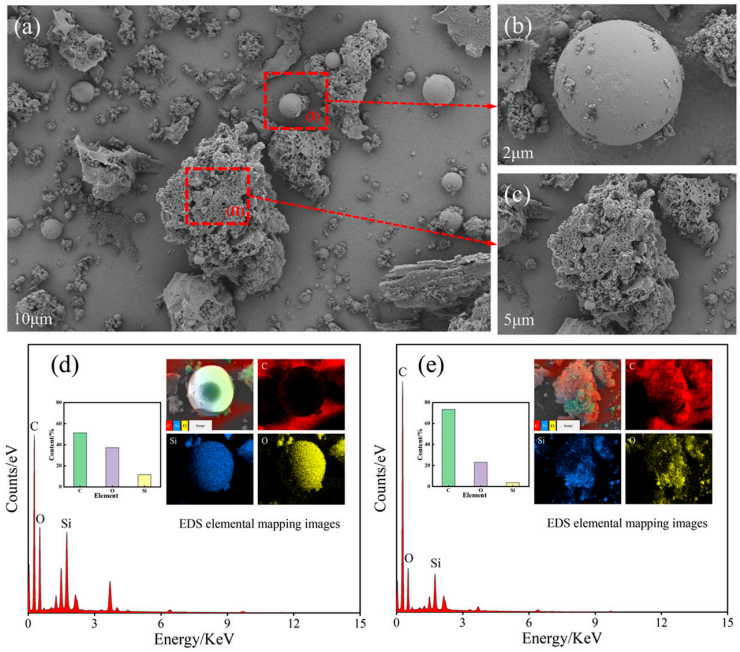

Figure 4. SEM–EDS images of coal gasification fine slag. (**a**) surface morphology; (**b**) spherical particle morphology; (**c**) fluffy granular morphology; (**d**) EDS spectrum of spherical particles; (**e**) EDS spectrum of fluffy granules.

2.3. Experimental Methods

2.3.1. Reagent Adsorption Experiments

The conditioning pretreatment process enables sufficient interaction between CGFS particles and the collector, thus promoting adsorption of the reagent on particle surfaces. To investigate the adsorption behavior of CGFS particles toward the collector under different feeding flow rates, ultraviolet–visible (UV–Vis) absorption spectra of the conditioned slurry obtained at different feeding flow rates were measured using a UV–Vis spectrophotometer (Evolution 201, Thermo Fisher Scientific, Waltham, MA, USA).

Sudan III was used as a dye to form a complex with kerosene for coloration, which amplifies the effect of reagent concentration on solution color and facilitates the acquisition of UV absorption spectra [28,32,33]. Kerosene and Sudan III were co-dissolved in anhydrous ethanol to prepare a homogeneous and stable dyed-kerosene mixture, which was subsequently mixed with deionized water to prepare kerosene solutions with different concentrations. The absorbance of each solution was measured to establish a calibration curve, and the fitted results are shown in Figure 5, where the predicted values exhibit good agreement with the experimental values, with a correlation coefficient exceeding 0.99.

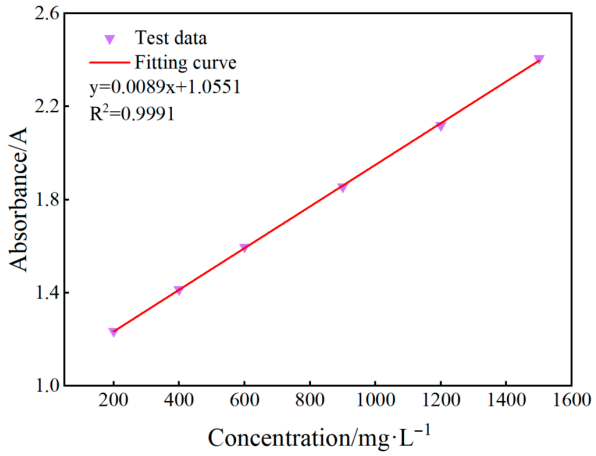

Figure 5. Calibration curve of kerosene absorbance.

During the conditioning pretreatment, 8.5 g of kerosene and 0.14 g of Sudan III were dissolved in 50 mL of anhydrous ethanol and mixed with 50 mL of deionized water to prepare the collector solution. The collector was introduced into the dosing pipe of the conditioning equipment at a constant rate using a dropper and entered the machine through self-aspiration to mix with the slurry. At the outlet of the conditioning equipment, 50 mL of slurry was collected and centrifuged to achieve phase separation, after which the supernatant was collected to measure the residual reagent concentration and calculate the amount of reagent adsorbed on the particle surfaces. For each operating condition, three parallel experiments were conducted, and the final results were reported as the average values. The formula for reagent adsorption on the particle surface is as follows:

$$q(\mathrm{mg/g}) = \frac{(C_o - C_e)V}{m} \quad (1)$$

In the equation, q represents the reagent adsorption (mg/g), C_o and C_e denote the initial kerosene concentration (mg/L) and the kerosene concentration in the supernatant after equilibrium (mg/L), respectively, V is the volume of the solution (L), and m is the mass of solids in the solution (g).

2.3.2. Zeta Potential Measurements

The conditioning pretreatment process can alter the surface charge characteristics of CGFS particles. To investigate the variation in surface charge of CGFS particles in the slurry under different feeding flow rates, zeta potential measurements were conducted for samples obtained after conditioning at different feeding flow rates using a zeta potential analyzer (Brookhaven Instruments, Holtsville, NY, USA).

At the outlet of the conditioning machine, 50 mL of slurry was collected. Centrifugation was then performed at a speed of 500 rpm for a duration of 5 min. The supernatant was then carefully extracted for zeta potential measurements. For each operating condition, three parallel experiments were performed, and 5 mL of supernatant was used for each measurement, with the final results reported as the average values.

2.3.3. Wrap Angle Measurements

The conditioning pretreatment process can influence the CGFS surface hydrophobicity. To investigate the variation in particle surface hydrophobicity in the slurry under different feeding flow rates, a laboratory-constructed particle–bubble attachment test platform was employed to evaluate the adhesion behavior of conditioned particles on the surface of a single bubble. This testing method is referred to as the wrap angle measurement.

At the outlet of the conditioning device, 50 mL of slurry was collected and freeze-dried using a freeze dryer to preserve the surface state by minimizing capillary forces and reagent redistribution during drying, thereby maintaining the spatial distribution of the adsorbed collector. Subsequently, 1 g of the freeze-dried sample was used for the wrap-angle experiment. The sample was uniformly added into a glass cell filled with deionized water, and a magnetic stirrer was operated at 1000 rpm for 2 min to ensure full particle dispersion. A micro-syringe was used to generate a bubble with a diameter of approximately 3 mm beneath the liquid surface. The stirring speed was then reduced to 250 rpm and maintained for 1 min, after which images were captured using a high-speed camera. The wrap angle was defined with the center of the bubble as the vertex. When measuring samples obtained under different feeding flow rate conditions, the bubble size was kept approximately the same for each group of experiments. Three parallel experiments were conducted for each operating condition, and the final results were taken as the average value.

2.3.4. XPS Analysis

The conditioning pretreatment process can influence the surface functional groups of CGFS samples. To investigate the variations in surface functional groups of CGFS particles in the slurry under different feeding flow rates, X-ray photoelectron spectroscopy (K-Alpha, Thermo Fisher Scientific, Waltham, MA, USA) was employed to analyze the surface functional group composition of samples after conditioning at different operating conditions.

At the outlet of the conditioning equipment, 100 mL of slurry was collected, and to preserve the post-conditioning state of the samples after drying, freeze-drying was performed using the freeze dryer. The freeze-dried samples were then subjected to XPS analysis to characterize the surface functional groups. For each test, 1 g of the freeze-dried sample was placed in a constant-temperature vacuum environment for surface composition analysis. High-resolution spectra were acquired using an Al Kα radiation source with a scanning step size of 0.1 eV. All spectra were charge-corrected using the C 1s peak at 284.8 eV as the reference. Background subtraction was performed using the Shirley method, and peak fitting was conducted using a Gaussian–Lorentzian mixed function with the full width at half maximum constrained within a reasonable range for each chemical state. The obtained XPS data were post-processed and analyzed using Avantage5.99 software.

2.3.5. Flotation Experiments

The gasification slag samples were introduced to conditioning experiments using the confined-turbulence pulp conditioning equipment at a slurry concentration of 100 g/L. To investigate the effect of feeding flow rate on the conditioning process, conditioning experiments were conducted at four feeding flow rates of 0.85 m^3/h, 0.56 m^3/h, 0.42 m^3/h, and 0.33 m^3/h, corresponding to slurry residence times of 40 s, 60 s, 80 s, and 100 s, respectively. The flow rate was regulated by adjusting the operating frequency of the slurry pump. During conditioning, the impeller rotational speed was fixed at 2000 rpm. Kerosene was used as the collector at a dosage of 9 kg/t and was introduced into the machine through the reagent dosing pipe via self-aspiration. After the conditioning pretreatment, the slurry was collected from the outlet of the machine for subsequent flotation experiments and characterization analyses. The calculation formula for the relationship between feeding flow rate and residence time is given as follows:

$$t(\mathrm{s}) = \frac{V}{Q} \times 3600 \tag{2}$$

where t represents the slurry residence time (s), V denotes the internal volume of the conditioning device (m^3), and Q represents the feeding flow rate (m^3/h).

The flotation experiments were conducted using a laboratory flotation column with a volume of 1 L, with aeration provided by an air pump. Methyl isobutyl carbinol (MIBC) was used as the frother at a dosage of 13 kg/t. The slurry subjected to conditioning pretreatment was mixed with the frother and then introduced into the flotation column to ensure sufficient mixing between the slurry and the frother. The air pump was then activated to supply air at a flow rate of 0.15 m^3/h, and after 10 s of aeration, froth scraping was initiated. The total flotation time was 5 min, after which the concentrates and tailings were separately filtered, dried, and weighed to calculate the yield, and the ash content of each sample was measured and recorded. The final flotation performance was evaluated using the combustible recovery of the flotation concentrate, which was calculated according to the following equation:

$$RUC(\%) = \frac{M_C(100 - A_C)}{M_F(100 - A_F)} \times 100\% \tag{3}$$

where RUC represents the combustible recovery, M_C and M_F denote the yields (%) of the concentrate and the feed, respectively, while A_C and A_F represent the ash contents (%) of the concentrate and the feed, respectively.

2.3.6. Flotation Kinetic Experiments

The operating procedure of the flotation rate experiments was the same as that of the above flotation tests. Methyl isobutyl carbinol (MIBC) was used as the frother at a dosage of 13 kg/t, and the aeration rate was maintained at 0.15 m^3/h. During the froth scraping process, concentrate products were collected at flotation times of 30 s, 1 min, 2 min, 3 min, and 5 min, respectively. The collected concentrate and tailings were then filtered, dried, and weighed, and the ash content of each sample was measured and recorded.

To investigate the evolution of flotation behavior with flotation time, six flotation kinetic models were employed to fit and analyze the cumulative combustible recovery obtained from the flotation rate experiments. The flotation kinetic models are listed in Table 3. Data fitting and calculations were carried out using 1stOpt8.0 software, based on the Levenberg–Marquardt algorithm combined with a universal global optimization algorithm. The maximum ultimate combustible recovery (ε_∞), flotation rate constant (k), and correlation coefficient (R^2) were determined for the flotation rate experiments [34].

Table 3. Six flotation kinetic models.

No.	Model	Formula
1	Classical first-order model	$\varepsilon = \varepsilon_\infty[1 - \exp(-kt)]$
2	First-order model with rectangular distribution	$\varepsilon = \varepsilon_\infty\{1 - \frac{1}{kt}[1 - \exp(-kt)]\}$
3	Fully mixed reactor model	$\varepsilon = \varepsilon_\infty(1 - \frac{1}{1+t/k})$
4	Improved gas/solid adsorption model	$\varepsilon = \varepsilon_\infty(\frac{kt}{1+kt})$
5	Second-order kinetic model	$\varepsilon = \frac{\varepsilon_\infty{}^2 kt}{1+\varepsilon_\infty kt}$
6	Second-order model with rectangular distribution of floatabilities	$\varepsilon = \varepsilon_\infty\{1 - \frac{1}{kt}[\ln(1+kt)]\}$

3. Results and Discussion

3.1. Analysis of Reagent Adsorption Behavior

The relationship between reagent adsorption amount and conditioning time during the conditioning process is shown in Figure 6. The results indicate that as the conditioning time increases from 40 s to 80 s, the amount of reagent adsorbed on particle surfaces increases from 5.79 mg/g to 6.94 mg/g, suggesting that prolonged conditioning enhances effective contact between particles and reagents, and promotes reagent adhesion on particle surfaces, thereby improving reagent adsorption. However, when the conditioning time is further extended to 100 s, the reagent adsorption amount decreases to 6.59 mg/g, indicating that excessively long conditioning times may induce over-shearing, leading to the reagent desorption from particle surfaces and the reduction in reagent adsorption. The above phenomenon is attributed to the fact that when the conditioning time is short, the mechanical energy and shear action input by the flow field are insufficient. This fails to provide adequate kinetic energy to rupture the hydration film on the particle surface, resulting in a limited mechanical scrubbing effect on the hydrophilic slimes. Consequently, the particle surface fails to expose sufficient hydrophobic sites, thereby restricting the effective adsorption and spreading of the collector. With an appropriate extension of the residence time, the collision frequency and interaction intensity between particles and reagents in the strong turbulent flow field are significantly enhanced. The high-intensity shear force effectively detaches the slime coatings, enabling the reagents to adsorb and spread more thoroughly on the particle surface. However, when the residence time is excessively long, over-conditioning occurs. The excessive mechanical shear force not only fails to further intensify the modification, but instead destroys the already formed hydrophobic oil film, causing the reagents originally adsorbed on the particle surface to desorb.

3.2. Zeta Potential Analysis

Zeta potential measurements were performed on the samples treated with different conditioning times, and the results are shown in Figure 7. At a conditioning time of 40 s, the zeta potential of the system was −18.94 mV. As the conditioning time increased to 80 s, the zeta potential decreased to −28.14 mV, indicating a progressive increase in the electronegativity of the system. When the conditioning time was further extended to 100 s, the zeta potential shifted to −24.53 mV, reflecting a certain degree of reduction in the system's electronegativity.

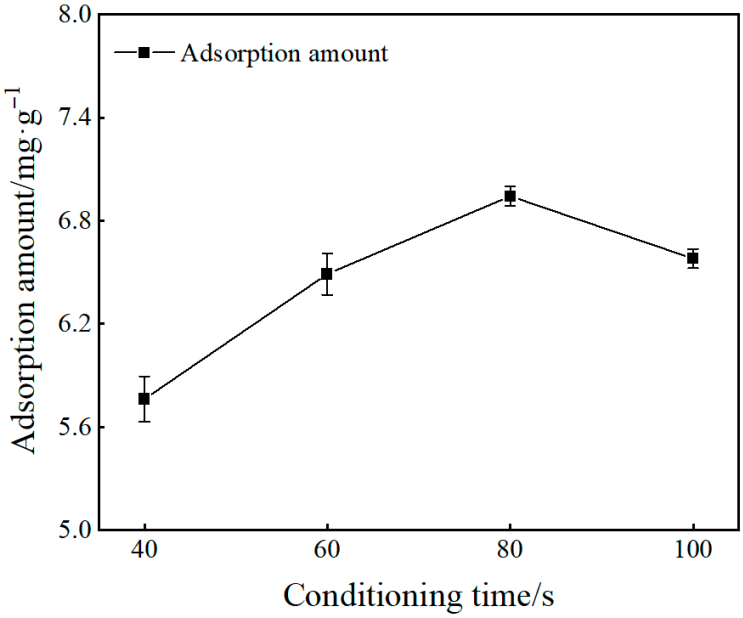

Figure 6. Effect of conditioning time on reagent adsorption amount.

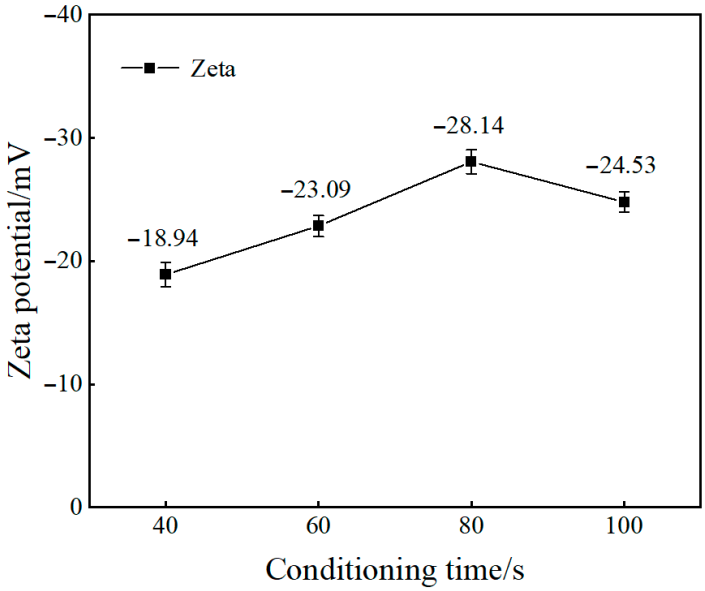

Figure 7. Effect of conditioning time on zeta potential.

3.3. Wrap Angle Analysis

Wrap angle measurements were performed on samples obtained after conditioning at different conditioning times, and the variation in wrap angle with conditioning time is shown in Figure 8. The angle between the orange lines represents the value of the angle. The results indicate that the wrap angle initially increases and then slightly decreases with increasing conditioning time. When the conditioning time increases from 40 s to 80 s, the wrap angle increases from 90° to 107°, indicating that during the conditioning pretreatment, the strong turbulent environment and high-shear action effectively enhance the interactions between particles and bubbles. However, when the conditioning time is further extended to 100 s, the wrap angle decreases to 102°, implying that excessively long conditioning times may lead to over-shearing, causing reagent desorption and a consequent reduction in surface hydrophobicity.

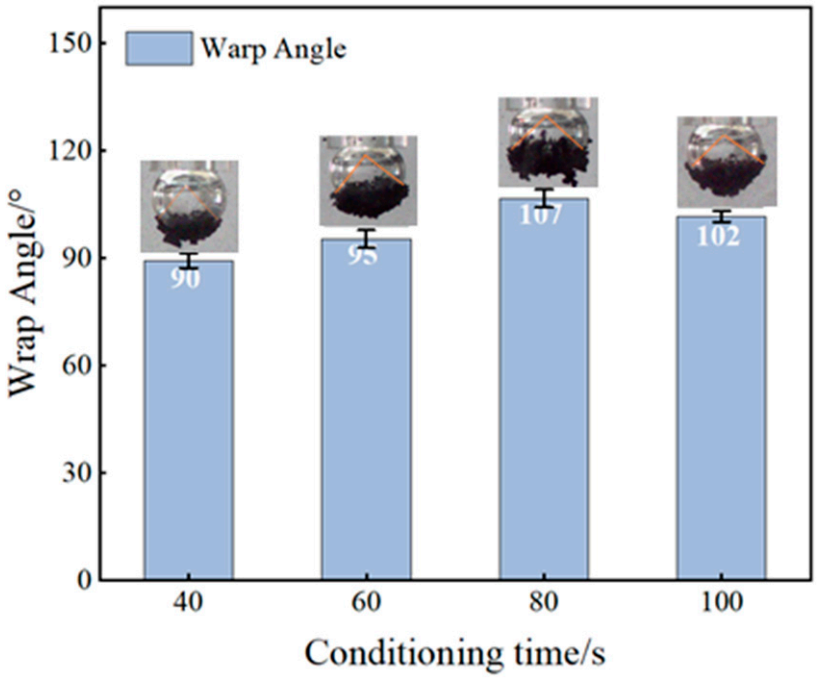

Figure 8. Effect of conditioning time on wrap angle.

3.4. XPS Results Analysis

X-ray photoelectron spectroscopy (XPS) was employed to analyze and compare the variations in surface functional groups between the conditioned samples obtained under different conditioning times and the untreated raw sample, and the corresponding results are shown in Figure 9, where Figure 9a represents the untreated raw sample, and Figure 9b–e correspond to samples conditioned for 40 s, 60 s, 80 s, and 100 s, respectively. All spectra were charge-corrected using the C–C binding energy at 284.8 eV, and peak deconvolution was performed to resolve three types of functional groups, namely C–C, C–O, and C=O. As summarized in Table 4, the relative area fraction of C–C in the raw sample shown in Figure 9a is 65.42%, while the total proportion of oxygen-containing functional groups accounts for 34.58%, indicating a relatively high content of surface oxygen functionalities. As shown in Figure 9b–e, after conditioning pretreatment, the overall proportion of oxygen-containing functional groups decreases markedly, accompanied by an increase in the C–C fraction. As the conditioning time increases from 40 s to 80 s, the C–C proportion rises from 71.62% to 80.69%, while the total proportion of oxygen-containing functional groups decreases from 28.38% to 19.31%. It is hypothesised that conditioning pretreatment facilitated scrubbing and stripping of the polar oxide adsorption layer and overlying fine silt from the particle surface, exposing more hydrophobic sites. Simultaneously, the collector adsorbed and spread across the particle surface. When the conditioning time is further extended to 100 s, the C–C proportion decreases to 78.82%, and the total proportion of oxygen-containing functional groups increases to 21.18%, this is thought to result from excessive shear forces during prolonged conditioning, which partially diminished the surface modification effect. This phenomenon aligns with the aforementioned experimental findings.

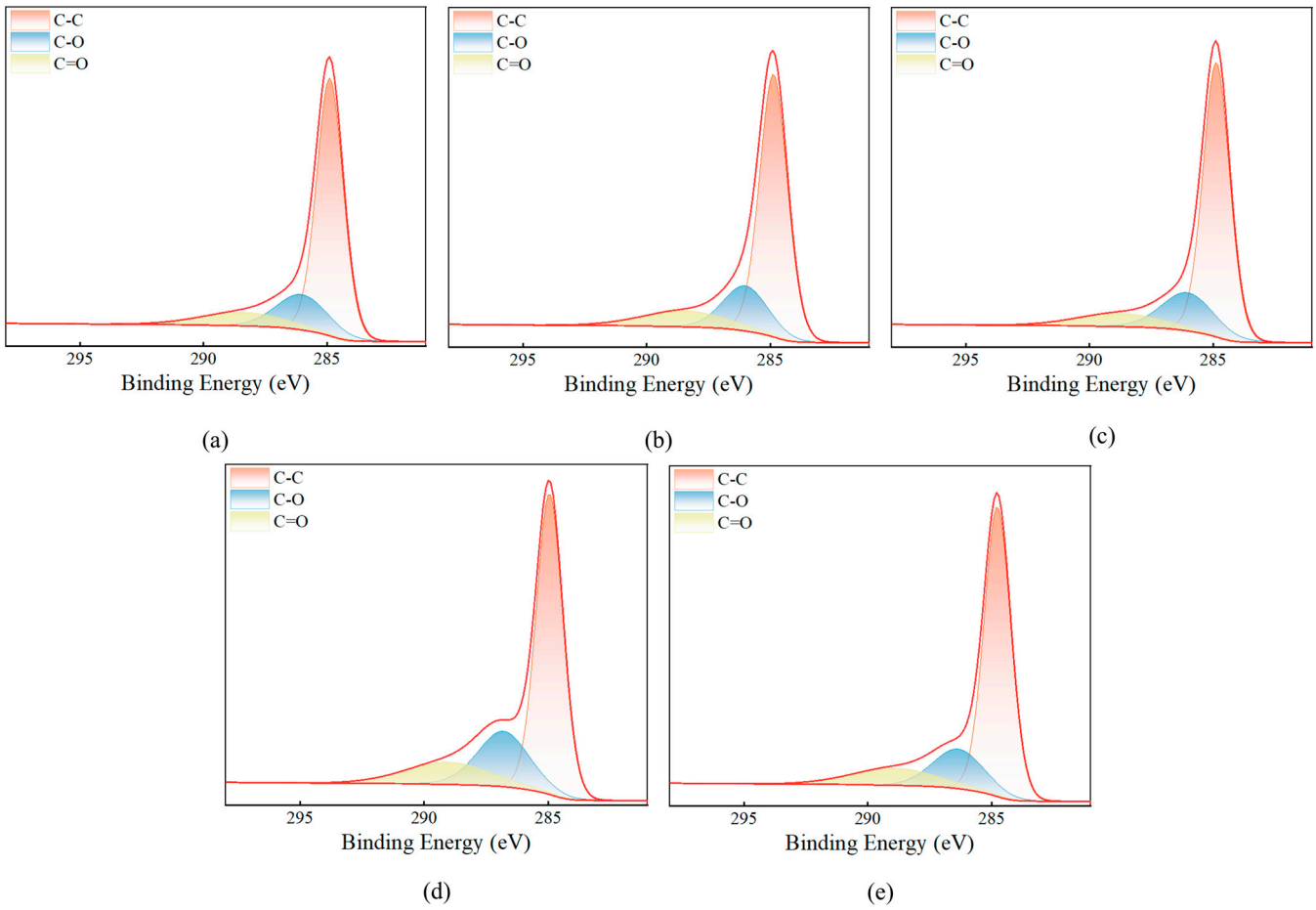

Figure 9. Comparison of XPS spectra of the raw sample and samples conditioned for different times. (**a**) raw sample; (**b**) 40 s; (**c**) 60 s; (**d**) 80 s; (**e**) 100 s.

Table 4. Surface functional group contents of the raw sample and samples after conditioning for different times.

Sample	Category	
	C–C/C–H	C–O; C=O
Untreated samples	65.42	34.58
Processed samples-40 s	71.62	28.38
Processed samples-60 s	75.34	24.66
Processed samples-80 s	80.69	19.31
Processed samples-100 s	78.82	21.18

3.5. Analysis of Flotation Experimental Results

Flotation experiments were conducted using conditioned CGFS at different conditioning times. The yield and ash content of concentrates are shown in Figure 10a, while those of the tailings are presented in Figure 10b. As the conditioning time increases from 40 s to 80 s, the yield of concentrates increases from 62.65% to 67.97%, and the ash content increases from 65.03% to 65.65%. Meanwhile, the ash content of the tailings increases from 90.74% to 94.05%, and the yield decreases from 37.35% to 32.03%. When the conditioning time is further extended to 100 s, the concentrate yield decreases to 64.91% and the ash content decreases to 64.95%, while the tailings ash content decreases to 92.14% and the yield increases to 35.09%. These flotation results indicate that increasing the conditioning time within an appropriate range is beneficial for enhancing flotation performance. However, excessively

long conditioning times lead to a deterioration in flotation performance, which is consistent with the results obtained from the preceding characterization and analysis experiments.

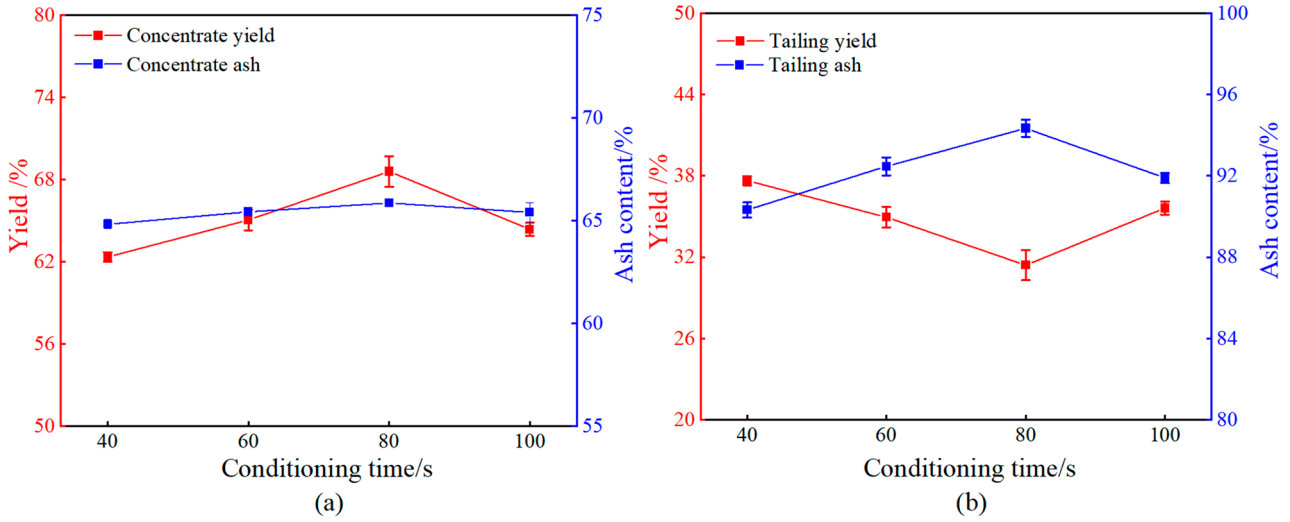

Figure 10. Effect of conditioning time on flotation performance. (**a**) flotation concentrate curve; (**b**) flotation tailings curve.

3.6. Analysis of Flotation Kinetic Experimental Results

The experimental results of CGFS flotation were fitted using flotation kinetic models, with the fitting results shown in Figure 11. All six kinetic models exhibit high fitting accuracy for the flotation kinetic data obtained at different conditioning times, and the fitting quality shows a gradual decreasing trend from Model 1 to Model 6. For all operating conditions, the fitting results obtained using Model 1 yield correlation coefficients (R^2) greater than 0.99, while those obtained using Model 6 also show R^2 values exceeding 0.98, indicating that the experimental data possess good kinetic fitting characteristics.

During the conditioning pretreatment process, the conditioning time has a significant influence on the maximum ultimate unburned carbon recovery (ε_∞) and the flotation rate constant (k) in gasification slag flotation, as summarized in Table 5. For all kinetic models, the fitted values of ε_∞ exhibit a trend of first increasing and then decreasing with increasing conditioning time, with the maximum value reached at 80 s. For a given operating condition, the fitted ε_∞ values increase progressively from Model 1 to Model 6, with similar values observed for Models 3–5. In theory, the maximum value of ε_∞ should be 100%. However, the fitted ε_∞ values obtained from Models 2–6 exceed 100%, which is physically unreasonable as the recoverable material yield cannot surpass the theoretical maximum of 100%. This indicates that these kinetic models are not entirely suitable for describing the flotation behaviour of this system under the current kinetic conditions. In contrast, Model 1 yields ε_∞ values below 100% for all operating conditions while giving rise to the highest R^2 value, making it more appropriate to characterize the flotation kinetics of the present system. Under this model, the variation trend of the maximum ultimate unburned carbon recovery is consistent with that shown in Figure 11. The flotation rate constant (k) reflects the variation in unburned carbon recovery during the flotation process, and its dependence on conditioning time follows a trend similar to that of $\varepsilon\infty$, initially increasing and then decreasing, with an optimal value obtained at 80 s, indicating that the highest unburned carbon recovery can be achieved at this conditioning time.

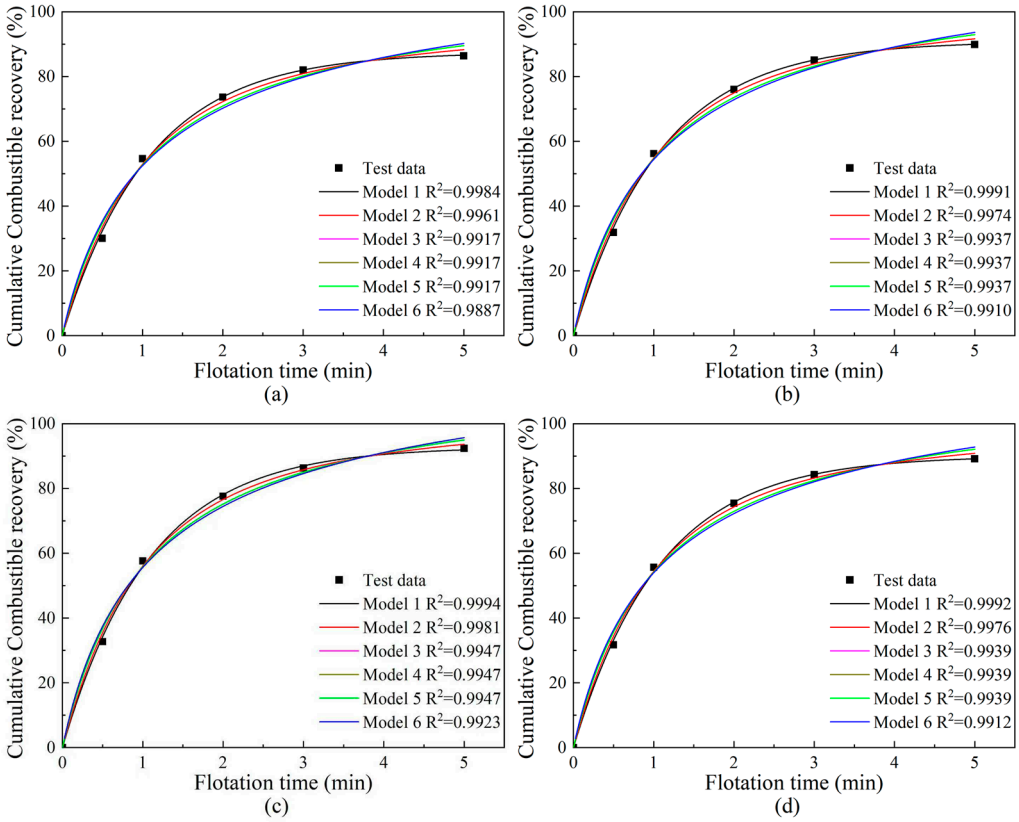

Figure 11. Influence of six flotation kinetic models on fitting the experimental data at different conditioning times (**a**) 40 s; (**b**) 60 s; (**c**) 80 s; (**d**) 100 s.

Table 5. Effect of conditioning time on the kinetics of unburned carbon recovery during flotation.

Model		Conditioning Time			
		40 s	**60 s**	**80 s**	**100 s**
Model 1	ε_∞, %	87.48	90.88	92.87	90.07
	k, s^{-1}	0.9144	0.9191	0.9199	0.9202
	R^2	0.9984	0.9991	0.9994	0.9992
Model 2	ε_∞, %	99.55	103.39	105.77	102.45
	k, s^{-1}	1.761	1.7637	1.7698	1.7681
	R^2	0.9961	0.9974	0.9981	0.9976
Model 3	ε_∞, %	108.56	112.74	115.22	111.69
	k, s^{-1}	1.0516	1.0653	1.0641	1.0619
	R^2	0.9917	0.9937	0.9947	0.9939
Model 4	ε_∞, %	108.57	112.78	115.22	111.71
	k, s^{-1}	0.9316	0.9384	0.9398	0.9413
	R^2	0.9917	0.9937	0.9947	0.9939
Model 5	ε_∞, %	108.57	112.76	115.22	111.71
	k, s^{-1}	0.0077	0.0083	0.008	0.0084
	R^2	0.9917	0.9937	0.9947	0.9939
Model 6	ε_∞, %	120.29	124.92	127.71	123.72
	k, s^{-1}	1.8596	1.8642	1.8672	1.8711
	R^2	0.9887	0.991	0.9923	0.9912

For CGFS, the core industrial objective is to maximize residual carbon recovery, thereby achieving solid waste reduction and resource utilization. Concentrate yield serves as a

process indicator, while the key parameter for evaluating the intensification effect of conditioning units lies in cumulative combustible recovery. The results of flotation kinetics obtained at different conditioning times were fitted using a first-order kinetic model, and the cumulative combustible recovery under each operating condition is shown in Figure 12. The results indicate that, with increasing conditioning time, the cumulative combustible recovery of CGFS during the flotation process exhibits a trend of first increasing and then decreasing. As the conditioning time increases from 40 s to 80 s, the cumulative combustible recovery rises from 86.37% to 92.45%, whereas a further increase in conditioning time to 100 s leads to a decrease in cumulative combustible recovery to 89.19%. This behavior demonstrates that increasing the conditioning pretreatment time within an appropriate range is beneficial for intensifying the flotation process and enhancing the recovery of combustible matter from CGFS, while excessively long conditioning times deteriorate flotation performance and result in reduced combustible recovery, which is consistent with the trends observed in the preceding experimental results.

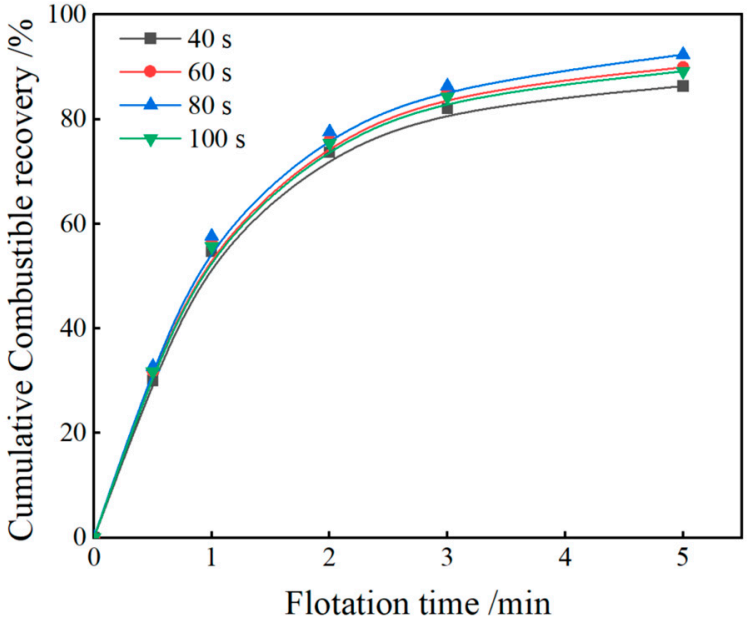

Figure 12. Effect of conditioning time on cumulative combustible recovery.

4. Conclusions

A conditioning–flotation system was developed in this study, employing a confined-turbulence pulp conditioning machine (CTPCM) as the core unit to intensify the CGFS flotation. A series of characterization tests and conditioning–flotation experiments were conducted to investigate the effects of the conditioning pretreatment process on the flotation performance of CGFS.

The characterization results demonstrate that as the conditioning pre-treatment time increased from 40 s to 80 s, the reagent adsorption capacity rose from 5.79 mg/g to 6.94 mg/g, the Zeta potential decreased from −18.94 mV to −28.14 mV, and the contact angle increased from 90° to 107°. Meanwhile, XPS analysis revealed that the content of oxygen-containing functional groups on the particle surface decreased from 28.38% to 19.31%, whereas the surface C–C content increased from 71.62% to 80.69%. These findings indicate that appropriately extending the conditioning time can effectively enhance the collision and adhesion between the reagent and the particles, thereby improving the collision-attachment interactions of the reagent on the particle surface. However, when the conditioning time was further extended to 100 s, the reagent adsorption effect on the particle surface was somewhat weakened compared to the 80 s condition. This is attributed to the fact that an

excessively low feed flow rate coupled with a prolonged conditioning time led to the deterioration of the turbulent flow field environment within the apparatus, thereby diminishing the surface modification effect to a certain extent.

Flotation experiments demonstrated that extending the conditioning time from 40 s to 80 s increased the concentrate yield from 62.65% to 67.97% and the tailings ash content from 90.74% to 94.05%, while the cumulative combustible recovery rose from 86.37% to 92.45%; simultaneously, the flotation kinetic rate constant k increased from 0.9144 to 0.9199, and ε_∞ grew from 87.48% to 92.87%. When the conditioning time was further extended to 100 s, the flotation performance exhibited a declining trend. These flotation results are highly consistent with the aforementioned characterization and testing outcomes. These findings indicate that, within a certain range, extending the conditioning pre-treatment time enhances particle–reagent interactions, thereby effectively improving the flotation performance of CGFS. However, an excessively prolonged conditioning time may cause reagent desorption from the particle surfaces, which consequently diminishes the intensification effect of the conditioning process on flotation. In summary, the optimal surface modification effect is achieved under the conditioning operating conditions of a 0.42 m^3/h feed flow rate and an 80 s residence time, which maximizes the combustible recovery and achieves the effective separation of carbonaceous matter and ash components in CGFS. Compared to traditional flotation methods, this study improves reagent utilization efficiency and combustible recovery levels through the intensified conditioning process, thereby reducing processing costs to a certain extent.

Author Contributions: Conceptualization, S.Y. and H.H.; Methodology, S.Y. and X.L.; Software, S.Y., X.L. and H.H.; Validation, S.Y. and D.L.; Formal analysis, S.Y.; Investigation, S.Y. and H.H.; Resources, S.Y., X.Y. and H.W.; Data curation, S.Y., X.L., D.L., H.H., J.R. and H.W.; Writing—original draft, S.Y.; Writing—review & editing, X.L., D.L., J.R., H.Z. and H.W.; Visualization, X.L., D.L., X.Y., H.Z. and H.W.; Supervision, X.L., J.R., X.Y., H.Z. and H.W.; Project administration, J.R., X.Y., H.Z. and H.W.; Funding acquisition, J.R., X.Y., H.Z. and H.W. All authors have read and agreed to the published version of the manuscript.

Funding: This research was funded by the National Natural Science Foundation of China (No. U21A20325, U25B6009, No. 52225405).

Data Availability Statement: Data will be made available upon request.

Conflicts of Interest: The authors declare no conflicts of interest.

References

1. Li, B.; Rahman, M.M.; Haneklaus, N. Assessing China's energy transition pathway: Insights from the synergistic effects of key drivers. *Energy Strategy Rev.* **2024**, *55*, 101528. [CrossRef]
2. Zhang, C.; Zhou, K.; Yang, S.; Shao, Z. On electricity consumption and economic growth in China. *Renew. Sustain. Energy Rev.* **2017**, *76*, 353–368. [CrossRef]
3. Liu, H.; Guo, W.; Fan, Z.; Huang, F.; Liu, S. Comparative life cycle energy, water consumption and carbon emissions analysis of deep in-situ gasification based coal-to-hydrogen with carbon capture and alternative routes. *J. Clean. Prod.* **2023**, *426*, 139129. [CrossRef]
4. Kong, L.; Tan, X.; Gu, B.; Yan, H. Significance of achieving carbon neutrality by 2060 on China's energy transition pathway: A multi-model comparison analysis. *Adv. Clim. Change Res.* **2023**, *14*, 32–42. [CrossRef]
5. Xu, G.; Zang, L.; Schwarz, P.; Yang, H. Achieving China's carbon neutrality goal by economic growth rate adjustment and low-carbon energy structure. *Energy Policy* **2023**, *183*, 113817. [CrossRef]
6. Ren, L.; Ding, L.; Guo, Q.; Gong, Y.; Yu, G.; Wang, F. Characterization, carbon-ash separation and resource utilization of coal gasification fine slag: A comprehensive review. *J. Clean. Prod.* **2023**, *398*, 136554. [CrossRef]
7. Guo, F.; Chen, L.; Li, Y.; Zhu, Y.; Jia, W.; Guo, Y.; Guo, S.; Zhang, Y.; Wu, J. Review on the attribute cognition and carbon-ash-water separation of coal gasification fine slag. *Sep. Purif. Technol.* **2023**, *320*, 124121. [CrossRef]

8. Xuan, W.; Gao, J.; Yan, S.; Liu, Z.; Sun, K.; Peng, B.; An, H. Physicochemical transformation of gasification slags with different residue carbon contents during sintering/melting process. *Fuel* **2024**, *368*, 131540. [CrossRef]
9. Zhao, X.; Yang, K.; He, X.; Zhang, L. Overview of the triple attributes and their connections of coal gasification slag in China: Resources, materials, and environment. *Fuel* **2025**, *400*, 135646. [CrossRef]
10. Lv, B.; Chai, X.; Deng, X.; Jiao, F.; Fang, C.; Xing, B. Recovery of residual carbon from coal gasification fine slag by a combined gravity separation-flotation process. *J. Environ. Manag.* **2023**, *348*, 119351. [CrossRef]
11. Han, R.; Zhang, N.; Zhou, A.; Li, Z.; Qu, J.; Wang, H. Enhancing flotation recovery of residual carbon from gasification waste by mixing hydrophobic powder with diesel as collector. *Particuology* **2024**, *89*, 211–217. [CrossRef]
12. Guo, Y.; Wu, J.; Guo, F.; Zhang, Y.; Yuan, S.; Du, C.; Chen, J.; Lin, M. Recycling of flotation residual carbon from coal gasification fine slag through thermal combustion reaction: Insight into the spatial and temporal multi-scale evolution of typical heavy metals. *Fuel* **2025**, *381*, 133378. [CrossRef]
13. Han, R.; Zhou, A.; Zhang, N.; Li, Z.; Cheng, M.; Chen, X.; Nan, T. Effective separation of coal gasification fine slag: Role of classification and ultrasonication in enhancing flotation. *Int. J. Min. Sci. Technol.* **2024**, *34*, 867–880. [CrossRef]
14. Tang, Y.; Yang, W.; Chen, S.; Shen, Z.; Feng, Q.; Zhang, Q. A green and biodegradable depressant for efficient flotation separation of smithsonite from calcite. *Sep. Purif. Technol.* **2026**, *380*, 135562. [CrossRef]
15. Gao, F.; Dong, L.; Xue, Z.; Cai, S.; Fan, M.; Hao, B.; Fan, P.; Bao, W.; Wang, J. Dodecylamine enhanced coal gasification fine slag flotation and its molecular dynamics simulation. *Miner. Eng.* **2023**, *203*, 108322. [CrossRef]
16. Guo, F.; Miao, Z.; Guo, Z.; Li, J.; Zhang, Y.; Wu, J. Properties of flotation residual carbon from gasification fine slag. *Fuel* **2020**, *267*, 117043. [CrossRef]
17. Zhang, N.; Cheng, M.; Han, R.; Li, Z.; Chen, S.; Zhu, Z.; Yu, Y.; Zhou, A. Innovative flotation separation considering pores blocking to facilitate residual carbon recovery from coal gasification fine slag. *Sep. Purif. Technol.* **2023**, *310*, 123254. [CrossRef]
18. Zhang, N.; Zhao, F.; Han, R.; Li, Z.; Zhu, Z.; Qu, J.; Wang, H.; Zhou, A. Resources recovery from coal gasification residue by combined hydrocyclone and vibrating screen and characterization of separated products. *Process Saf. Environ. Prot.* **2024**, *184*, 1272–1281. [CrossRef]
19. Dong, L.; Xue, Z.; Gao, F.; Yang, C.; Li, H.; Bao, W.; Wang, J.; Fan, P. Research on extraction of carbon from coal gasification fine slag using hydrophobic-hydrophilic separation: Efficient separation, molecular dynamics simulation, and model optimization. *Fuel* **2024**, *365*, 131180. [CrossRef]
20. Chen, R.; Wang, H.; Lin, B.; Li, D.; Zhang, B.; Ran, J.; Zhang, H. Mineralization interaction process between an air bubble and carbon or ash particles collected from coal gasification fine slag. *Fuel* **2025**, *394*, 135156. [CrossRef]
21. Xue, Z.; Dong, L.; Fan, M.; Yang, H.; Liu, A.; Li, Z.; Bao, W.; Wang, J.; Fan, P. Enhanced flotation mechanism of coal gasification fine slag with composite collectors. *Colloids Surf. A Physicochem. Eng. Asp.* **2022**, *641*, 128593.
22. Jiao, Y.; Yang, Z.; Han, X.; Wang, K.; Fang, C.; Zhao, Z.; Tang, W. Ultrasonication Improves the Flotation of Coal Gasification Fine Slag Residue. *Minerals* **2024**, *14*, 363. [CrossRef]
23. Chen, R.; Wang, H.; Li, D.; Liao, Y.; Tian, Q.; Su, W.; Li, L.; Zhang, H. Numerical and Experimental Study on the Colliding Flow Pulp Conditioning for the Separation Intensification of Unburned Carbon from Coal Gasification Slag. *Minerals* **2023**, *13*, 398. [CrossRef]
24. Liang, Y.; Wang, H.; Chen, R.; Li, D.; Tian, Q.; Li, L.; Zhang, H. Intensification of flotation separation process of residual carbon from coal gasification fine slag using ultrafine carbon particles conditioning. *Int. J. Coal Prep. Util.* **2024**, *44*, 2044–2059. [CrossRef]
25. Li, D.; Yan, X.; Wang, W.; Wang, H.; Zhou, R.; Yang, H.; Zhang, H. New insights into the intensification of collector adsorption on fine particles induced by flow field. *J. Mol. Liq.* **2022**, *365*, 120119. [CrossRef]
26. Li, X.; Sun, Z.; Wang, H.; Wang, L.; Yan, X.; Zhang, H.; Ran, J.; Liu, J. Particle motion under turbulent eddies: Inspiration for fine minerals flotation. *Chem. Eng. Sci.* **2025**, *301*, 120754.
27. Wang, H.; Yang, W.; Li, D.; Zhang, C.; Yan, X.; Wang, L.; Zhang, H. Enhancement of coal flotation using impact flow conditioning pulp. *J. Clean. Prod.* **2020**, *267*, 122124. [CrossRef]
28. Qin, Y.; Li, C.; Zhang, Y.; Zhang, H. Effect of nanobubbles on electrode material flotation: A comparative study of flotation kinetics. *Powder Technol.* **2026**, *467*, 121534.
29. Yu, Y.; Cheng, G.; Ma, L.; Huang, G.; Wu, L.; Xu, H. Effect of agitation on the interaction of coal and kaolinite in flotation. *Powder Technol.* **2017**, *313*, 122–128. [CrossRef]
30. Yang, L.; Li, D.; Zhu, Z.; Xu, M.; Yan, X.; Zhang, H. Effect of the intensification of preconditioning on the separation of unburned carbon from coal fly ash. *Fuel* **2019**, *242*, 174–183. [CrossRef]
31. Yang, S.; Hou, H.; Liu, J.; Yan, X.; Ran, J.; Wang, H.; Zhang, H. Enhancement of the pulp conditioning process for the flotation of coal gasification fine slag using turbulent forcing: Numerical and experimental investigation. *Powder Technol.* **2026**, *470*, 122008. [CrossRef]
32. Zhang, Z.; Ren, L.; Zhang, Y. Role of nanobubbles in the flotation of fine rutile particles. *Miner. Eng.* **2021**, *172*, 107140. [CrossRef]

33. Wang, X.; Han, Y.; Zhu, J.; Liu, L.; Wang, H.; Lin, Z.; Xia, S.; Wang, P. Effect of two-stage energy input on enhancing the flotation process of high-ash coal slime. *Physicochem. Probl. Miner. Process.* **2024**, *60*, 189958. [CrossRef]
34. Ni, C.; Bu, X.; Xia, W.; Peng, Y.; Xie, G. Effect of slimes on the flotation recovery and kinetics of coal particles. *Fuel* **2018**, *220*, 159–166. [CrossRef]

Disclaimer/Publisher's Note: The statements, opinions and data contained in all publications are solely those of the individual author(s) and contributor(s) and not of MDPI and/or the editor(s). MDPI and/or the editor(s) disclaim responsibility for any injury to people or property resulting from any ideas, methods, instructions or products referred to in the content.